nature physics

SUPPLEMENTARY INFORMATION

DOI: 10.1038/NPHYS2021

Unconditional Room Temperature Quantum Memory

M. Hosseini, G. Campbell, B. M. Sparkes, P. K. Lam and B. C. Buchler

[1]*Centre for Quantum Computation and Communication Technology, Department of Quantum Science, Research School of Physics and Engineering, The Australian National University, Canberra, ACT 0200 Australia*

S.1 THEORY

We start by deriving the equations of motion for Λ-GEM [S1]. We show that a Λ-system driven off-resonance by a strong coupling beam and a weak probe is equivalent to a two-level system driven by the weak probe. The lifetime of the equivalent two-level system is given by the ground state lifetime of the three-level atom and is therefore long lived [S2].

We solve the Maxwell-Bloch equations in the weak probe and far detuned regimes. We consider the three-level system depicted Fig.S1 (a) with a one photon detuning Δ, a classical coupling beam with Rabi frequency of Ω_c, and a weak quantum signal field $\hat{\mathcal{E}}$. The two-photon detuning $\delta(z,t)$ can be varied in time and be made linear with a magnetic or electric field $\delta(z,t) = \eta(t)z$. Fig.S1 (b) represents the equivalent two-level system.

We assume all the population to be in state $|1\rangle$ initially ($\sigma_{11} \simeq 1$). One difference between this off-resonance scheme and electromagnetically induced transparency (EIT) [S3], is that in steady state, and under normal experimental conditions, the atoms are not fully pumped by the coupling field to the level $|1\rangle$. To ensure that this occurs, an initial pumping step is required. From the Heisenberg/Maxwell equations in the weak probe regime and in a moving frame at the speed of light, we obtain

$$
\begin{aligned}
\dot{\hat{\sigma}}_{13} &= -(\gamma + \gamma_0/2 + i\Delta)\hat{\sigma}_{13} + ig\hat{\mathcal{E}} + i\Omega_c\hat{\sigma}_{12} + \hat{F}_{13} \\
\dot{\hat{\sigma}}_{12} &= -(\gamma_0 + i\delta(z,t))\hat{\sigma}_{12} + i\Omega_c^*\hat{\sigma}_{13} + \hat{F}_{12} \\
\frac{\partial}{\partial z}\hat{\mathcal{E}} &= i\mathcal{N}\hat{\sigma}_{13}
\end{aligned} \tag{1}
$$

where $\mathcal{N} = \frac{gN}{c}$ is the effective linear atomic density and N is the total number of atoms in the interaction volume. The Langevin operators $\hat{F}_{13}$ and $\hat{F}_{12}$ account for noise arising from spontaneous emission γ and ground state decoherence γ_0 respectively. It is possible that, in some regimes, these noise terms could result in noise being added to the states stored in the quantum memory. In a linear regime, where we assume the probe is very weak, these terms only add noise to the state that is required to maintain the Heisenberg uncertainty between conjugate observables in the presence of some passive loss [S4]. This is analogous to loss on a beamsplitter which introduces vacuum fluctuations. This simple noise behaviour means that we can ignore the Langevin noise terms in our modelling, then add the right amount of vacuum noise to the observables to correct for the efficiency of the memory. When the interaction time is small compared to the time between collisions of atoms we can also ignore the population redistribution terms, so that we simply assume that once the atoms are prepared in state $|1\rangle$, they stay there. modelling

S.1.1 Adiabatic elimination and far off-resonance approximation We adiabatically eliminate fast excited state fluctuations by assuming $\frac{\partial}{\partial t}\hat{\sigma}_{13} \ll \gamma$, or equivalently, $1/T \ll \gamma$ [S5], where T is the fastest time-scale of the system. We also assume a large one-photon detuning compared to the spontaneous emission rate ($\Delta \gg \gamma$). By solving the Maxwell equation for the probe field and substituting this back into the equation of motion for $\hat{\sigma}_{13}$ we can show that $1/dT \ll \gamma$ and $\Delta \gg \gamma d$, where d is the optical depth of the medium, are sufficient conditions to eliminate the excited state when the atomic density is larger than 1. This is due to the collective coupling between the optical modes and the many-atom state. Assuming the coupling beam amplitude to be real and $\Delta \neq 0$, combining the above three equations yields

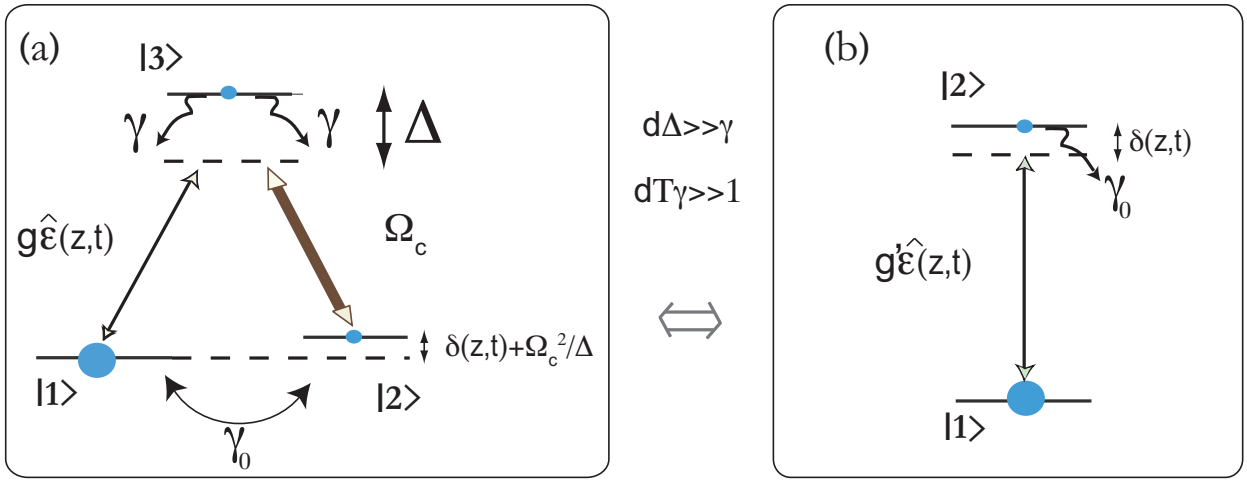

Figure S1: (a) Level structure of the three-level atom. (b) Equivalent two-level system.

$$\begin{aligned}\dot{\hat{\sigma}}_{12} &= (-\gamma_0 + i\delta(z,t) - i\frac{\Omega_c^2}{\Delta})\hat{\sigma}_{12} - i\frac{g\Omega_c}{\Delta}\hat{\mathcal{E}} \\ \frac{\partial}{\partial z}\hat{\mathcal{E}} &= \frac{ig\mathcal{N}}{\Delta}\hat{\mathcal{E}} + i\frac{\mathcal{N}\Omega_c}{\Delta}\hat{\sigma}_{12}.\end{aligned} \tag{2}$$

We can always choose a frame where the speed of light in the medium is normalised by the refractive index term $i\frac{gN}{\Delta}$ and can also choose the coupling beam frequency to match the light shift term $\frac{\Omega_c^2}{\Delta}$. With these two simplifications, we reach

$$\begin{aligned}\dot{\hat{\sigma}}_{12} &= -(\gamma_0 + i\delta(z,t))\hat{\sigma}_{12} - i\frac{g\Omega_c}{\Delta}\hat{\mathcal{E}} \\ \frac{\partial}{\partial z}\hat{\mathcal{E}} &= i\frac{\mathcal{N}\Omega_c}{\Delta}\hat{\sigma}_{12}.\end{aligned} \tag{3}$$

The equations for the two-level atomic system [S6] are

$$\begin{aligned}\dot{\hat{\sigma}}_{12} &= -(\gamma_{12} + i\delta'(z,t))\hat{\sigma}_{12} - ig'\hat{\mathcal{E}} \\ \frac{\partial}{\partial z}\hat{\mathcal{E}} &= i\mathcal{N}'\hat{\sigma}_{12},\end{aligned} \tag{4}$$

which are formally equivalent to the above Raman situation, if we set $\mathcal{N}' = \mathcal{N}\frac{\Omega_c}{\Delta}$ and $\gamma = \gamma_0$.

The equations of motion for this system can be solved in the Fourier domain where it has been shown previously that one can construct a normal mode description of the system [S7].

S.1.2 Frequency shift. Storage in a two-level or three-level GEM system can result in frequency shifts of the light [S6], [S8] resulting mostly from the interaction of the reradiated light field with resonant atoms. The amplitude of the optical field inside the memory inversely scales by k, the spatial frequency of the atomic polarisation in the propagation direction. As shown in [S6], the evolution of the stored light pulse through k-space is given by $k = \eta t$. In particular, when the interaction time is short in comparison with the input pulse duration or when small inhomogeneous broadening is applied, a time dependent phase shift appears in our numerical simulations.

Numerical simulation reveals a clear k dependent frequency shift. These results are plotted in Fig. S2. The observed frequency shift here is linearly dependent on the inverse of k so that the longer the light is stored, or the larger the atomic frequency gradient, the smaller the linear frequency shift.

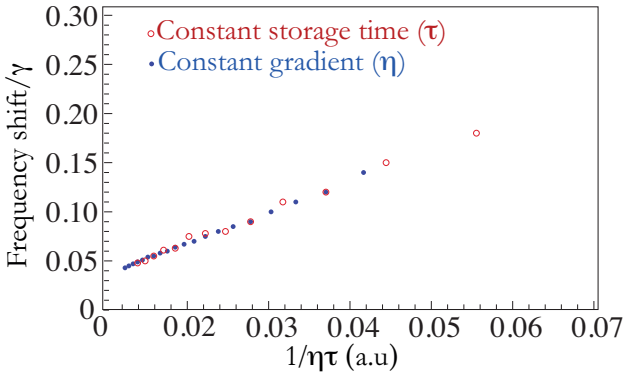

Figure S2: Numerical simulation showing the frequency shift of the output field for various values of $1/\eta\tau$. The frequency shift is shown for two cases. Red points correspond to frequency shift with constant storage time (τ) varying η, and blue points are corresponding to constant η while τ is changing. The rate γ is the excited state linewidth.

A simple frequency shift can also be applied deliberately by varying the external DC field or changing the frequency of the coupling field at read out. We use this external control to eliminate in any linear frequency shift from our pulse storage. Specifically, we introduce an offset magnetic field to cancel out the inherent frequency shift effect of the memory. The frequency shift in two and three-level CRIB systems has been theoretically studied in Ref. [S8]. It was shown that a three-level CRIB system mediated by π pulses can show linear and nonlinear phase modulation in the echo field under some conditions, particularly short interaction times and high optical depth. We note here that our experiment does not operate in this regime and indeed, we have not observed any non-linear frequency shift in our system.

S.2. EXPERIMENTAL METHODS

The experiment was conducted using a cylindrical cell (length and diameter were 20 cm and 25 mm, respectively) cell containing ^{87}Rb atoms mixed with 0.5 Torr Kr buffer gas in order to increase the time of flight of the atoms inside the beam. The experimental setup is shown in Fig.S3 (a). We split the Ti:sapphire laser beam, blue detuned typically by 1-3 GHz from the $F_g = 2$ to $F_e = 1$ transition of the ^{87}Rb D1 line, into two beams. One beam is phase-modulated to produce sidebands that are separated from the carrier by 6.835 GHz (i.e. the ground-state hyperfine splitting of ^{87}Rb). This beam then goes through a cavity that is resonant with the +6.8 GHz sideband to filter out the carrier and -6.8 GHz sideband.

The second laser beam was used as the coupling beam. Both the coupling and the signal fields pass through AOMs to shape their temporal profiles. The signal beam was collimated to a diameter of 6mm while the control field covers almost the entire cell cross section. The signal pulses and control beam were then combined with the same linear polarisation using another cavity that is resonant with the signal field. The control and signal fields were converted to circular polarisation and sent into the gas cell. The temperature of the cell was controllably tuned to $\sim 80^o$C using a bifilar resistive heater wound around the cell. After the memory, the control field was filtered out using another cell containing ^{85}Rb atoms. Homodyne detection of the signal beam was performed

after the filtering cell. The fringe visibility of the homodyne was 97% and quantum efficiencies of the detectors were ∼90%. With the 70% transmission of the ^{85}Rb cell, the end-to-end detection efficiency was ∼56%.

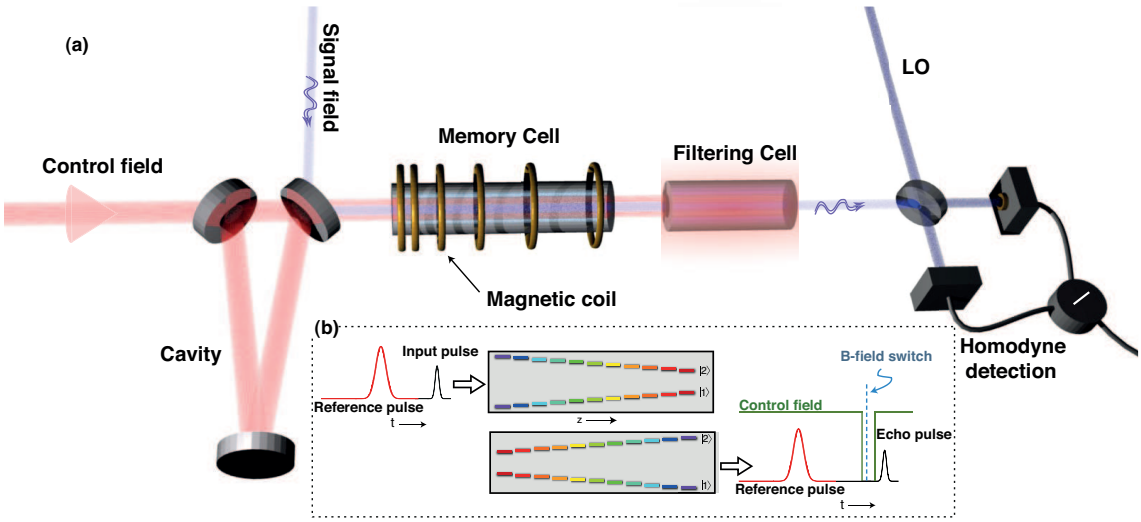

Figure S3: (a). Schematic experimental setup showing the control and the signal fields being mixed on a mode cleaner cavity and sent to the memory. The control field is filtered out using a ^{85}Rb gas cell and homodyne detection is performed on the signal after interfering with the local oscillator (LO) on a 50/50 beam splitter. (b). Schematic of pulse sequences during the experiment period. The reference pulse with different frequency is shown as a red pulse that is not absorbed and is used to track the phase of the input and echo pulses. The control field is switched off for 1 μs after storage of the pulse. The echo is emitted after switching the gradient field and turning on the control field.

S.2.1. Magnetic field To create the frequency gradient, two specially wound magnetic coils surrounding the cell are used to produce opposing linearly varying Zeeman shifts along the cell [S9]. Switching the current between these coils created a switchable atomic frequency gradient in our

storage medium. To recall the pulse, one coil is switched off (in 0.5 μs) and one is switched on (in 2.5 μs). The typical value of the gradient field is 20 mG/cm, which gives an atomic frequency gradient of 28 kHz/cm. Using an additional solenoid we also applied a DC magnetic field of 6 G. The cell and coils are surrounded with $\mu-$metal to reduce the influence of the Earth's magnetic field.

S. 2.2. Gas cell filtering Using a ^{85}Rb vapour cell after the memory cell, more than 60 dB suppression of the control field can be obtained. The temperature of the filtering cell was set to $\sim$110 ^{o}C. As it can be seen from Fig.S4, if the control field is detuned by about 3 GHz from $F_g = 2$ to $F_e = 2$ it would be close to resonant with a ^{85}Rb transition and will therefore be absorbed. The control field leakage through the filtering cell is well below the local oscillator power and has a different frequency and spatial mode from the signal beam. It therefore does not contaminate the homodyne detection results. On the other hand, the signal field is well away from any transition and the absorption is low. The filtering cell attenuates the signal beam by 30% which is mostly due to the lack of an anti-reflection coating on the windows of the cell and the presence of some ^{87}Rb atoms in the cell. This loss could be reduced by using a pure ^{85}Rb isotope with anti-reflection coated windows. When the control field was guided through the filtering gas cell at $T > 100^o$C we observed purple fluorescence. Since the control and signal fields have different spatial modes one can also use a single mode fibre (SMF) to separate the two beams, the problem associated with this method is that the control field leakage through the fibre can be significant. Using a gas cell filter together with a SMF or cavity can suppress the control field down to single photon level [S10].

S. 2.3. Phase detection To determine the phase of each pulse, we used a strong reference pulse as shown in Fig.S3 (b). The reference pulse has a fixed phase relation to the signal but differs in frequency by more than the broadened Raman linewidth and therefore is not absorbed. By fitting the phase of the reference pulse we can accurately infer the phase of the input and echo pulses.

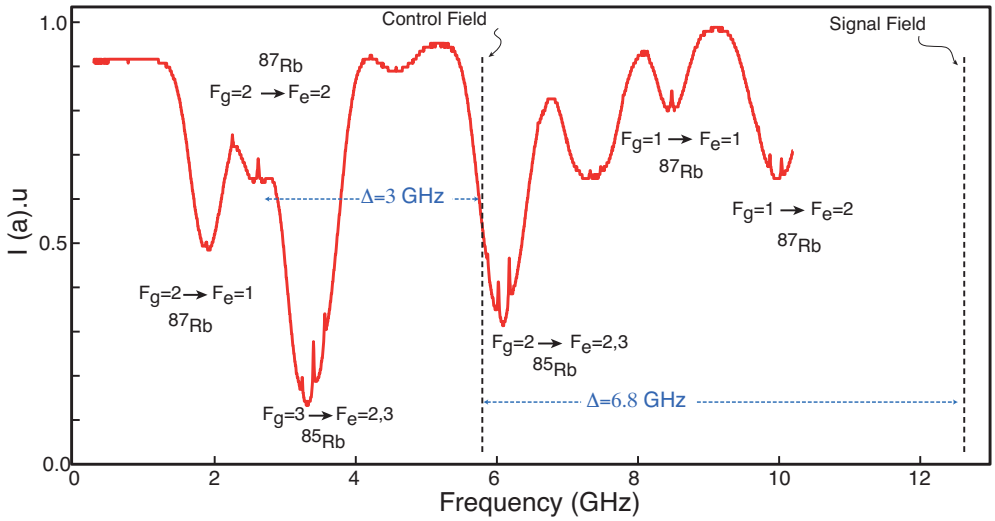

Figure S4: Saturation absorption of vapour cell containing natural mixture of Rb showing different D1 line transitions of ^{85}Rb and ^{87}Rb. The dashed lines shows where the frequency of the control and the signal fields are located on this spectrum.

We have an error of $\Delta\theta = 29$ mrad in the fitting of the pulse phase. For a given amplitude (A), this phase error can be translated into an added variance which in all cases was less than 0.04 and therefore negligible.

We have found that there is a constant phase relation between the input and echo signals. This has been removed from the echo signal during the post processing. To obtain quadrature values for different phases, we allow the phase of the local oscillator to slowly drift. This thermal drift is much slower than the single-shot measurement time and therefore provides an even distribution of measurement phase. Ensemble quadrature values for each phase was obtained by taking quadrature values within bins with width of $2\pi/100$.

S.3. QUANTUM MEASUREMENTS

S.3.1. Photon distribution The Poissonian distributions shown in Fig. 2 E and F (in the main paper) are theoretical fits using only the mean photon number calculated by summing over the

relevant photon probability distribution. To obtain the photon distributions for the no-cloning and quantum limits we assume our memory is a source of Gaussian noise that is added equally to the phase and amplitude quadratures. We add just enough noise to each quadrature to reach these limits then reconstruct the photon number distributions as we did before. In the case of the no-cloning limit we assume the added quadrature variance of $2\eta - 1$ where the η is the efficiency of the memory. The added noise in the case of the quantum limit can be shown to be 2η (see supplementary information in [S11]. This assumption is truly valid only if the input state is a coherent state which is the case for the state plotted in Fig. 2 F.

The iterative maximum-likelihood (MaxLik) method was used to reconstruct the density matrix elements of various states obtained from a set of balanced homodyne measurements [S12]. Assuming a particular density matrix ρ, one can evaluate the probability of acquiring a particular set of measurement results. The purpose of the MaxLik method is to find a density matrix that maximises the probability of obtaining the given experimental data set. In practice, the iteration algorithm is executed with the density matrix in the photon number (Fock) representation. Since the Hilbert space of optical states is of infinite dimension, the implementation of the algorithm requires its truncation so that the Fock terms above a certain threshold are excluded from the analysis.

S.3.2. Fidelity The overlap fidelity between two optical states with Gaussian quadrature distributions [S13] can be written as

$$\mathcal{F} = 2e^{-\frac{2\delta_x^2}{V_{in}^+ + V_{out}^+} - \frac{2\delta_y^2}{V_{in}^- + V_{out}^-}} / (\sqrt{(V_{in}^+ V_{out}^- + 1)(V_{in}^- V_{out}^+ + 1)} - \sqrt{(V_{in}^+ V_{in}^- - 1)(V_{out}^+ V_{out}^- - 1)}) \quad (5)$$

where $\delta_{x/y}$ is the distance between the two states in the phase space along the amplitude (x) and phase (y) axes. $V_{in/out}^{\pm}$ are the amplitude (+) and phase (-) quadrature variances of the input and output states. To calculate the optimal memory performance (small black lines in Fig. 4A) we use the input parameters in Table S1. We then find the distance between the input and output states and the output noise by assuming a beamsplitter relation for the memory, where the transmissivity of the beamsplitter is the efficiency of the memory. This limit therefore assumes that the memory is just a source of passive loss and the atomic processes add no extra noise.

The Gaussian no-cloning limit is obtained if $\delta_x = \delta_y = 0$ and $V_{out}^{\pm} = V_{in}^{\pm} + 1$. For coherent states we have $V_{in}^{\pm} = 1$, and the maximum cloning fidelity is therefore 2/3 [S**?**]. Using a non-Gaussian cloner one can obtain slightly higher fidelity for 1-to-2 cloning of coherent states, $\mathcal{F}_{NG-cloning}$ =0.6826 [S14].

$\langle N \rangle$	V_{in}^{+}	V_{in}^{-}	η	$\mathcal{F}$
0.67	1.20	1.10	0.86	0.98
3.41	1.14	1.40	0.83	0.93
12.0	1.63	4.52	0.67	0.76
16.3	1.57	2.08	0.77	0.82
22.4	2.03	7.51	0.74	0.68

Table S1: Experimental parameter table. Mean photon number $\langle N \rangle$, input variances ($V_{in}^{\pm}$), efficiency (η) and fidelity ($\mathcal{F}$) of different optical states used in Fig. 4 A and B.

S.3.3. TV diagram The transfer coefficient (T) and conditional variances (V) for two orthogonal quadratures are defined, respectively, as $T^{\pm} = \eta/(1 + V_{out}^{\pm} - V_{in}^{\pm})$ and $V_{cv} = (1 - T^{\pm})V_{out}^{\pm}$ from which the two quantum limits of $V_{cv}^{+} \times V_{cv}^{-} \leq 2$ and $T^{+} + T^{-} \leq 1$ are obtained. T-V characterisation of a quantum device is state independent, however as it is seen in the Fig. 3 A, the measured conditional variance is different for different states. The quantum efficiency of the detectors (90%), fringe visibility of the homodyne (97%) as well as the loss of the signal through the filtering cell (30%) have been taken into account in calculating the conditional variances by extrapolating the variances of the input and output to the state prior to these losses. This provides the truest account of the performance of the memory. If we did not account for the losses, an overestimate in the performance would result since we would have underestimated the signal-to-noise ratio of the original input state.

[S1] Hetet, G. Quantum memories for continuous variable states of light in atomic ensembles. PhD thesis, The Australian National University (2008).

[S2] Balabas, M. V. *et al.* High quality anti-relaxation coating material for alkali atom vapor cells. *Opt. Exp.* **18**, 5825–5830 (2010).

[S3] Fleischhauer, M. & Lukin, M. Dark-state polaritons in electromagnetically induced transparency. *Physical Review Letters* **84**, 5094–5097 (2000).

[S4] Hetet, G., Peng, A., Johnsson, M. T., Hope, J. J. & Lam, P. K. Characterization of electromagnetically-induced-transparency-based continuous-variable quantum memories. *Phys. Rev. A* **77**, 012323–16 (2008).

[S5] Gorshkov, A. V. & et al. *Phys. Rev. Lett.* **98**, 123601–4 (2007).

[S6] Hetet, G., Longdell, J. J., Alexander, A. L., Lam, P. K. & Sellars, M. J. Electro-optic quantum memory for light using two-level atoms. *Phys. Rev. Lett.* **100**, 023601–4 (2008).

[S7] Hetet, G., Longdell, J. J., Sellars, M. J., Lam, P. K. & Buchler, B. C. Multimodal properties and dynamics of gradient echo quantum memory. *Phys. Rev. Lett.* **101**, 203601–4 (2008).

[S8] Moiseev, S. A. & Arslanov, N. M. Efficiency and fidelity of photon-echo quantum memory in an atomic system with longitudinal inhomogeneous broadening. *Phys. Rev. A* **78**, 023803–14 (2008).

[S9] Hétet, G. *et al.* Photon echoes generated by reversing magnetic field gradients in a rubidium vapor. *Opt. Lett.* **33**, 2323–2325 (2008).

[S10] Jin, X.-M. & et al. Quantum interface between frequency-uncorrelated down-converted entanglement and atomic-ensemble quantum memory. *arXiv:1004.4691v1 [quant-ph]* (2010).

[S11] Hedges, M., Longdell, J., Li, Y. & Sellars, M. Efficient quantum memory for light. *Nature* **465**, 1052–1056 (2010).

[S12] Lvovsky, A. I. Iterative maximum-likelihood reconstruction in quantum homodyne tomography. *J. Opt. B: Quantum Semiclass. Opt.* **6**, S556–S559 (2004).

[S13] Jeong, H., Ralph, T. C. & Bowen, W. P. Quantum and classical fidelities for gaussian states. *J. Opt. Soc. Am. B* **24**, 355–362 (2007).

[S14] Cerf, N. J., Kruger, O., Navez, P., Werner, R. F. & Wolf, M. M. Non-gaussian cloning of quantum coherent states is optimal. *Phys. Rev. Lett.* **95**, 070501–4 (2005).